PERGAMON

Deep-Sea Research II 46 (1999) 77–108

DEEP-SEA RESEARCH
PART II

Temporal changes in eddy energy of the oceans

Detlef Stammer*, Carl Wunsch

Department of Earth, Atmospheric, and Planetary Sciences, Massachusetts Institute of Technology, Cambridge, MA 02139, USA

Received 29 August 1997; received in revised form 14 January 1998

Abstract

Insight into the sources of eddy energy in the ocean can be obtained by studying the degree and nature of its temporal changes. As a preliminary to a dynamical and modeling discussion, we provide a description of the changes in variability on the annual and interannual time scales as seen in the TOPEX/POSEIDON altimeter data and in current meter records with a focus on the North Atlantic and North Pacific Oceans. The patterns of change and corresponding ones in the wind stress are globally very variable and intricate, with few easy generalizations possible. Over most of the subtropical oceans and along major mean fronts, seasonal variations of the eddy energy are negligible. There are, however, regions that show a pronounced annual cycle in eddy energy, notably the northeastern Pacific, the northern and eastern North Atlantic, as well as the tropical oceans. In those locations a strong correlation of a time-varying altimetric eddy kinetic energy on annual and longer periods with wind stress forcing is found, and trends present in near-surface eddy kinetic energy can be related to drifts in meteorological wind stress fields (mean and storm tracks) over the four-year TOPEX/POSEIDON record. While the seasonal cycles in mooring data are found generally to agree with altimetry, the only statistically significant evidence for interannual trends in current meter data appears in the long duration eastern Atlantic site mooring near 33°N, 22°W.

1. Introduction

Oceanic variability is a direct or indirect response to a time-varying external atmospheric forcing and can be summarized as the result of (1) the direct response of the ocean to local and/or remote high-frequency surface forcing by the wind and

* Corresponding author. Tel.: 001 617 253 5259; fax: 001 617 253 4464; e-mail: detlef@lagoon.mit.edu.

0967-0645/99/$ – see front matter
PII: S0967-0645(98)00106-4

buoyancy effects, (2) dynamical instability processes, including barotropic and baroclinic instability of the mean flow, (3) eddy generation by flow over topography, and (4) dynamical processes (meandering) in oceanic jets. Some of this variability is "eddy-like", but some represents basin and larger-scale changes and some would look quite different in a Lagrangian rather than an Eulerian frame (e.g., jet meandering).

Beginning with programs such as the Mid-Ocean Dynamics Experiment (MODE Group, 1978) in the 1970s, oceanic variability has been explored globally (see, e.g., Robinson, 1983; Dickson, 1989; Wunsch, 1997) using in situ instruments in both a descriptive and dynamical form. The variability has been described commonly in terms of relative and absolute energy levels, and in terms of frequency spectra. But the spatial and temporal coverage has remained too sparse for general conclusions in a highly inhomogeneous ocean, and the different physical processes underlying the variability have often remained obscure.

Because of the association of the most intense observed variability with western boundary currents, especially the Agulhas, Kuroshio and Gulf Stream, it has long been suggested that much of the observed eddy energy was generated in these regions. Technically, however, there have been difficulties in rationalizing the radiation of the motion into the oceanic interior (e.g., Pedlosky, 1977; Talley, 1983; Hogg, 1988). Despite those difficulties these currents, whether or not dynamically unstable or interacting with topography (including retroflection), remain likely sources of interior ocean eddy energy.

Gill et al. (1974) studied the conditions for the baroclinic instability of the oceanic interior circulation, and showed that regions such as the Atlantic North Equatorial Current are potentially unstable, and, in principle, would provide eddy source terms in the interior oceans. A field study [Fu et al., 1982], however, failed to confirm the hypothesis. Later observations also failed to produce unequivocal evidence for any simple baroclinic instability hypothesis in the open sea (e.g., Mercier and Colin de Verdiere, 1985).

Exploration of a second potential mechanism for the generation of an open-ocean mesoscale eddy field by fluctuating winds was pioneered by Frankignoul and Müller (1979) and Müller and Frankignoul (1981) who developed a linear stochastic model that predicts the spectral properties of the quasigeostrophic ocean response to prescribed wind stress curl spectra. Stochastic forcing provides a simple explanation for the existence and spatial structure of coherence maxima in terms of the forcing wavenumber spectrum (Lippert and Müller, 1995). But the predicted energy levels, while comparable to those seen in the quietest parts of the ocean, are much smaller than what is observed elsewhere. Furthermore, the simulated energy level depends on assumptions about friction processes and the power density spectrum of the sea surface winds at high frequencies and wavenumbers. Forcing by high-frequency winds (time scales from days to weeks) should generate predominantly barotropic Rossby waves (e.g., Willebrand et al., 1980), with relatively small velocity amplitudes. Fu and Smith (1996), using a general circulation model (GCM), show the excitation of barotropic Rossby waves by high-frequency wind fluctuations in specific regions, which coincide with high atmospheric variability, especially the northeastern and

southeastern Pacific Ocean. Large et al. (1991) found, in a flat bottom, quasigeostrophic model of the North Pacific, that the effect of the barotropic waves generated by high-frequency European Centre for Medium-Range Weather Forcasts (ECMWF) wind stress forcing was to produce a change in variability energy on the annual time scale of about $0.4\ \mathrm{cm^2\,s^{-2}}$.

Recent significant improvements in satellite altimetry and of high-resolution numerical models of the ocean have led to new insights into the nature of the ocean mesoscale in terms of the regional dependence of amplitude and spectral characteristics. Both fields indicate a close association of the observed eddy kinetic energy distributions with the (local) mean baroclinic flow (Beckmann et al., 1994; Stammer and Böning, 1996; Stammer, 1998). Observed open-ocean mesoscale wavenumber characteristics are generally consistent with geostrophic turbulence, and associated eddy scales are strongly correlated with the first-mode Rossby radius of deformation. All this supports the hypothesis that mean flow instabilities are the major source of eddy energy over most areas of the mid-latitude oceans.

But after 25+ years of study, there still remain many quantitative obscurities concerning the origin and impact on the general circulation of the mesoscale variability. Here we explore the idea that interannual and annual changes in the eddy field, if present and if conspicuously related to similar changes in the wind stress, permits us to draw inferences about the origins of the variability. We explore temporal changes in the variability spectra and energy levels – quantities, which hitherto have usually been treated as time invariant. The central data here are four years of TOPEX/POSEIDON (henceforth T/P) data, producing a nearly global, uniform data coverage. These data are supplemented by a compilation of long-term records of moored current meters. Our goal is a descriptive one; discussion of the theoretical and modeling implications is postponed to a second paper (Stammer et al., in preparation).

The altimetric data have been discussed in detail in numerous papers and reviewed in Wunsch and Stammer (1998). Because the altimetric measurements directly observe only the seasurface, one must determine the extent and nature of the corresponding subsurface motions.[1] Wunsch (1997) made a global compilation of current meter moorings having some suitability for determining the vertical structure of the velocity variability on a global basis. A qualitative conclusion is that the altimeter tends to reflect the movement of the main thermocline (as described by the first linear baroclinic mode), but the degree to which this is true is a function of position in the ocean. Large deviations from the norm do occur.

[1] The accuracy of the altimeter data at the annual period is not yet completely clear: the so-called em-bias correction to the altimeter data is directly dependent at lowest order on the estimated seastate. Because the ocean surface wave field shows a strong seasonal change, some of the apparent oceanic seasonal cycle in currents may, particularly in high-wind regions, be an artifact of an imperfect em-bias algorithm.

2. The interannual variability

2.1. Altimetry

Define the surface slope anomaly,

$$\gamma = \frac{\partial \eta'}{\partial s}, \tag{1}$$

where s is the along-track distance and η' is the anomaly of sea surface height relative to the four year mean. The time-mean eddy kinetic energy then follows as

$$K_E = (g/(2\Omega \sin(\phi)))^2 \langle \gamma^2 \rangle, \tag{2}$$

with ϕ being the latitude and $\langle \cdot \rangle$ indicating a time average. We employ here an equivalent slope variance

$$K_S = \sin^2(\phi) K_E \tag{3}$$

as a substitute for the geostrophic kinetic energy, as it can be computed without the equatorial singularity generated by the vanishing Coriolis parameter at the equator. A global view of K_S as it results from four years of T/P data is shown in Fig. 1a. Only observations from locations with water depths greater than 1000 m were used. Noise on scales smaller than 30 km was first removed from the η fields by low-pass filtering as described in Stammer (1997, 1998), and results were gridded subsequently onto a 2° geographical grid. The close relation between the geographic K_S distribution and the path of the mean baroclinic circulation – which is obvious in the figure – was studied in some detail in Stammer (1998).

To illustrate the degree to which the field displayed in Fig. 1a fluctuates between years, we show in Fig. 1b the difference in K_S estimated separately from year four minus year one of the T/P data; the percentage of the change relative to the mean is displayed in Fig. 1c. Variations are generally in the range of $\pm 20\%$ of the four-year mean value.[2] In the northern hemisphere the subtropical gyres gain energy over the four years, while the tropical Pacific and the subpolar regions of the North Pacific and North Atlantic lose eddy energy. The largest changes can be found along the path of the Kuroshio extension and in the western tropical Pacific, where the fourth year shows a decrease in eddy energy by more than 50% of the mean value, and it can be anticipated that eddy transports will vary accordingly (cf. Stammer, 1998). Changes in the southern hemisphere are not so dramatic nor as spatially coherent. The Indian Ocean exhibits a growth in eddy energy in the east, while its tropical and western portions became quieter.

To interpret such changes, one needs to distinguish the variability expected from the statistical fluctuations of a temporally stationary (wide-sense) process in which the

[2] To focus on spatially coherent changes, both Fig. 1b and c were filtered to remove all grid-scale energy before plotting.

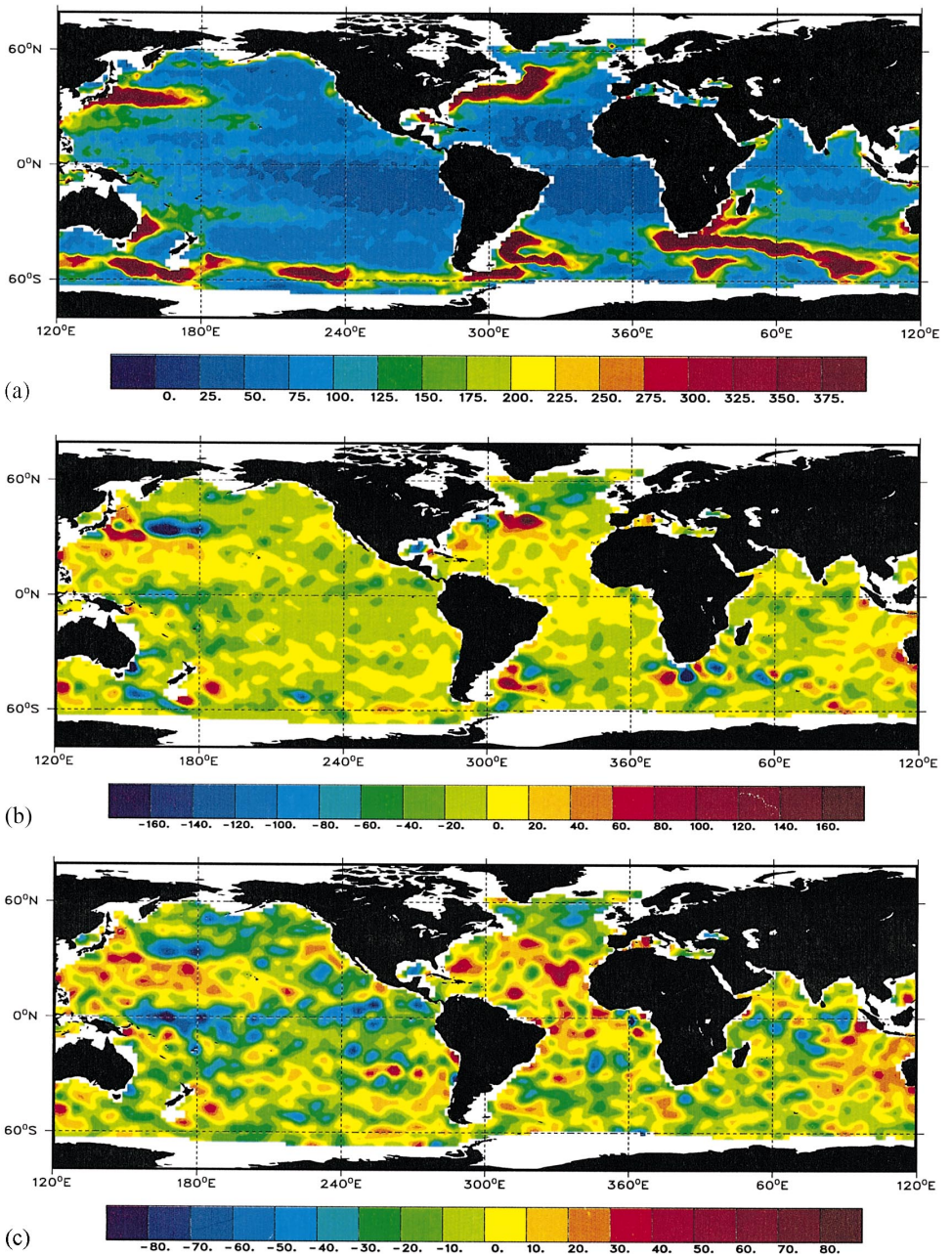

Fig. 1. (a) K_S from four years of TOPEX/POSEIDON alongtrack data over water depths greater than 1000 m and gridded on 2° grid. An assumption of isotropy was used, which leads to positive biases in regions of strong anistropic fields, such as the western boundary current extensions; see Wunsch (1997). (b) Differences of K_S estimates obtained separately from year four minus year one. (c) Same as as (b), but normalized by field shown in (a). Point changes by a factor of two are within the approximate values expected from a time-stationary random process. Contour increments are 25 cm^2/s^2, 20 cm^2/s^2, and 10% in (a), (b), and (c), respectively.

underlying statistics and physics are unchanged, from a change indicating a shift in physical and statistical conditions. A complete discussion of this problem is complex – involving the frequency/wavenumber spectrum – and is beyond the scope of this paper; the following is offered here as a useful approximation. Consider any physical variable, $\xi(t)$, which is supposed to have zero mean, and assume that we are able to compute a sequence of one year mean-square values from daily samples over different years, j:

$$\Delta^2_{\xi\xi}(j) = \frac{1}{365}\sum_{t=1}^{365} \xi^2(t + 365(j-1)). \tag{4}$$

How much variability would one expect to find in $\Delta^2_{\xi\xi}(j)$ from one year to the next?

First, suppose that $\xi(t)$ has a power density spectrum $\Phi_{\xi\xi}(\sigma)$. It follows from the Wiener–Khinchin theorem (Priestley, 1982) that

$$R_{\xi\xi}(\tau) \propto \int_0^\infty \Phi_{\xi\xi}(\sigma)\cos\sigma\tau\,\mathrm{d}\sigma. \tag{5}$$

From the altimeter, one can readily compute the global average slope spectrum $\Phi_{\xi\xi}(\sigma)$ (Fig. 2a) and the spectrum of slope-squared $\Phi_{\gamma^2\gamma^2}(\sigma)$ (Fig. 2b). An approximate analytical fit to the global $\Phi_{\gamma^2\gamma^2}(\sigma)$ spectrum is

$$\begin{aligned}\Phi_{\gamma^2\gamma^2}(\sigma) &= 2.6\times10^{-20}\left(\frac{\sigma}{2\pi}\right)^{-0.063}, \quad \frac{\sigma}{2\pi} \leqslant \frac{1}{62\,\mathrm{d}} \\ &= 3.9\times10^{-21}\left(\frac{\sigma}{2\pi}\right)^{-0.52}, \quad \frac{1}{62\,\mathrm{d}} \leqslant \frac{\sigma}{2\pi},\end{aligned} \tag{6}$$

becoming nearly "white" at periods beyond about 60 d.

Let $\xi(t)$ be a stationary time series of variance δ^2_ξ and autocorrelation $\rho_{\xi\xi}(\tau)$. Eq. (5.3.5) of Priestley (1982) estimates the variance of a sample average, m, over N data points as

$$\frac{var(m)}{\delta^2_\xi} = \frac{1}{N}\sum_{\tau=-(N-1)}^{\tau=N-1}\left(1-\frac{|\tau|}{N}\right)\rho_{\xi\xi}(\tau). \tag{7}$$

Thus if $\xi(t)$ were white noise, $\rho_{\xi\xi}(\tau) = \delta(\tau)$, and one would expect the variance of a one-year average to be 1/365 of the variance of $\xi(t)$ itself. But the finite autocorrelation reduces the available degrees-of-freedom, and increases the variance (depending upon the sign of $\rho_{\xi\xi}(\tau)$, it could decrease). Taking $\xi(t) = \gamma^2(l)$, the squared-slope, and employing the spectrum in Eq. (6), to obtain $\rho_{\xi\xi}(\tau)$, we have

$$\frac{1}{N}\sum_{\tau=-(N-1)}^{\tau=N-1}\left(1-\frac{|\tau|}{N}\right)\rho_{\xi\xi}(\tau) \approx \frac{5.3}{365} = 0.014 = 0.12^2, \tag{8}$$

and thus one expects fluctuations in the annual averages of $\gamma^2(t)$ of about 10% of the mean energy. The annual averages of the global mean K_S are 121, 118, 119 and 116 $\mathrm{cm}^2/\mathrm{s}^2$ for each of the four years, which is smaller than the expected change and probably due to the deviations from the underlying statistical assumptions.

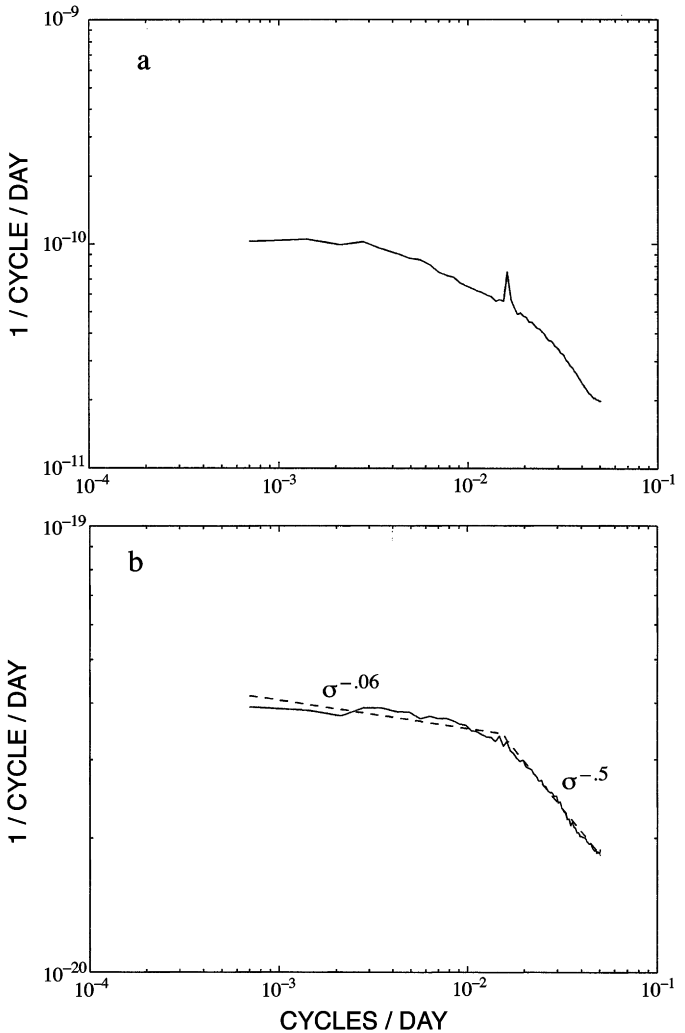

Fig. 2. (a) Frequency spectral density of four years of the global average of γ. The small peak is a residual alias of the semi-diurnal tides near 60 d period. (b) Frequency spectral density corresponding to a, except for γ^2, The tidal alias has essentially disappeared (the alias is a long wavelength phenomenon). Also shown is an analytical approximation to this spectrum which is nearly white for periods exceeding about 60 d.

The variations in regional altimetric eddy kinetic energy with time are shown in more detail in Fig. 3, which depicts timeseries of K_S estimated over various regions spanning 10° on a side in the North Atlantic. Curves represent monthly estimates, and dots show estimates from individual 10-d periods. Regional estimates of altimetric eddy kinetic energy have fewer degrees of freedom than does the global average, and one would expect a greater local interannual variability. On the other hand, local

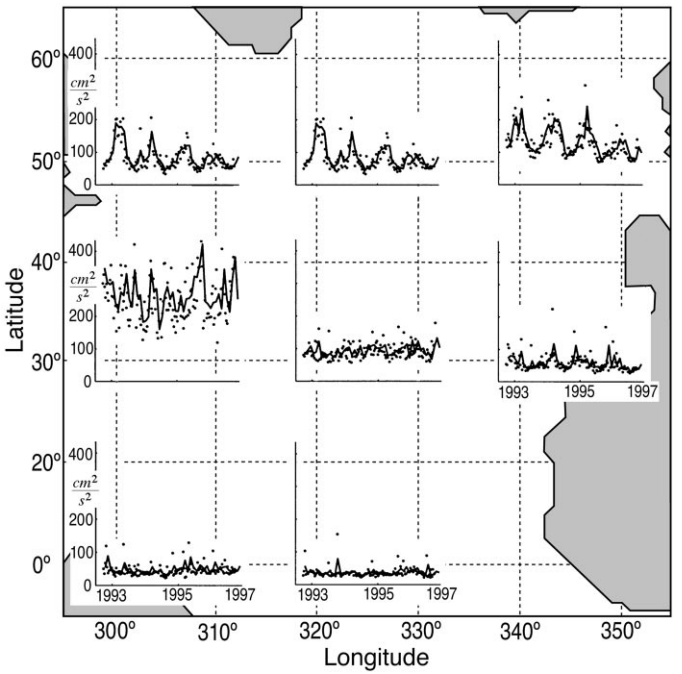

Fig. 3. Timeseries of monthly K_S estimated (in cm^2/s^2) in various regions spanning 10° on a side in the North Atlantic. The dots denote estimates from individual 10-d periods.

spectral estimates of γ^2 made in the 10° squares are similar in shape to the global average spectral estimate, presumably owing to a dominance of high wavenumber contributions. The expected fractional energy variability in any region thus be would approximately the same as for the global average.

If the regional average energies are asymptotically normal, then a two-sided 95% confidence limit would correspond to ± 1.96 standard deviations, which we take as ≈ 0.1 from Eq. (8). Thus fluctuations in annual average energies by more than about 20% are statistically unlikely. The appearance in Fig. 1 of large regions of change exceeding 30% suggests these are not simply the expected random variations of a stochastic process. Particular attention is called to the North Atlantic: the subpolar gyre and the Labrador Sea, as well as the Cape Verde Basin; and in the North Pacific: the Kuroshio Extension along 35°N, in the subpolar gyre, and especially the tropics. Later in the paper we will attempt to relate these changes to wind fluctuations although we will omit discussion of the tropical Pacific, which is strongly influenced by the ENSO cycle.

2.2. Current meters

Interannual fluctuations in kinetic energy have been known for some time from current meter measurements: Schmitz (1989) reported an approximately 50% change

in mesoscale energy at 28°N, 70°W (the so-called MODE site) as measured during a 200+ day interval in the mid-1970s when compared to a 20-month record 10 yr later.

As with the altimetry, we estimated a power density spectrum $\Phi_{uu}(\sigma)$ from a current meter record at 635 m in the North Pacific, which can be approximated by the analytical expression

$$\Phi_{uu}(\sigma) = 38\left(\frac{\sigma}{2\pi}\right)^{-0.4}, \quad \frac{\sigma}{2\pi} \leqslant \frac{1}{100\,\mathrm{d}}$$
$$= 0.04\left(\frac{\sigma}{2\pi}\right)^{-1.75}, \quad \frac{1}{100\,\mathrm{d}} \leqslant \frac{\sigma}{2\pi}. \tag{9}$$

Compared to the altimetric slope spectrum, the increased red nature at long periods produces an expected variability of an annual average of the pointwise subsurface current measurements from year to year that is larger than expected from the globally averaged altimetry.

This power density spectral estimate is that of the velocity, and not that of the velocity-squared, which would be analogous to $\Phi_{\gamma^2\gamma^2}$. To use it to find an estimate of the variability of annual average kinetic energy, we note that $\Delta^2_{\xi\xi}(j)$ in Eq. (4) is the zero-lag sample autocovariance; Priestley (1982, p. 327) gives an expression for its variance. Using that formula, the resulting numerically determined value of

$$\sum_{m=-\infty}^{\infty} \rho^2_{uu}(m) \approx 150 \tag{10}$$

produces

$$\{\langle(\Delta^2_{uu}(j) - \langle\Delta^2_{uu}(j)\rangle)^2\rangle\}^{1/2} \approx 0.9\delta^2_{uu}. \tag{11}$$

That is to say, one expects the rms variability of the mean-square energy computed over one-year samples of current meter measurements to be approximately equal to the energy itself and a factor of two fluctuation in local (point-wise) energy level is not unexpected. (Even if the u, v components are supposed uncorrelated, and the kinetic energy is formed as an average of two estimates with statistics such as that in Eq. (9), then one would expect the kinetic energy to very approximately equal to $1/\sqrt{2} \simeq 0.7$ of the total kinetic energy.) To the extent that the shape of Eq. (9) holds for the global current meter records (the energy level is immaterial), the change seen by Schmitz (1989) is consistent with the expected variability of a stationary process.

The remarkably long record from repeated deployments in the eastern North Atlantic described by Müller and Siedler [1992] however, may be evidence of a true secular shift. Fig. 4 depicts the record-mean kinetic energy through time. There has been a persistent loss in energy from the early 1980s to the values seen 10 years later. The origin of this shift, whether it is simply a movement of the Azores front (as suggested by Siedler et al., 1985) or represents a much larger scale change, cannot be ascertained with the data available. Although our results below suggest that the observed changes are due to large-scale adjustment of the ocean circulation to

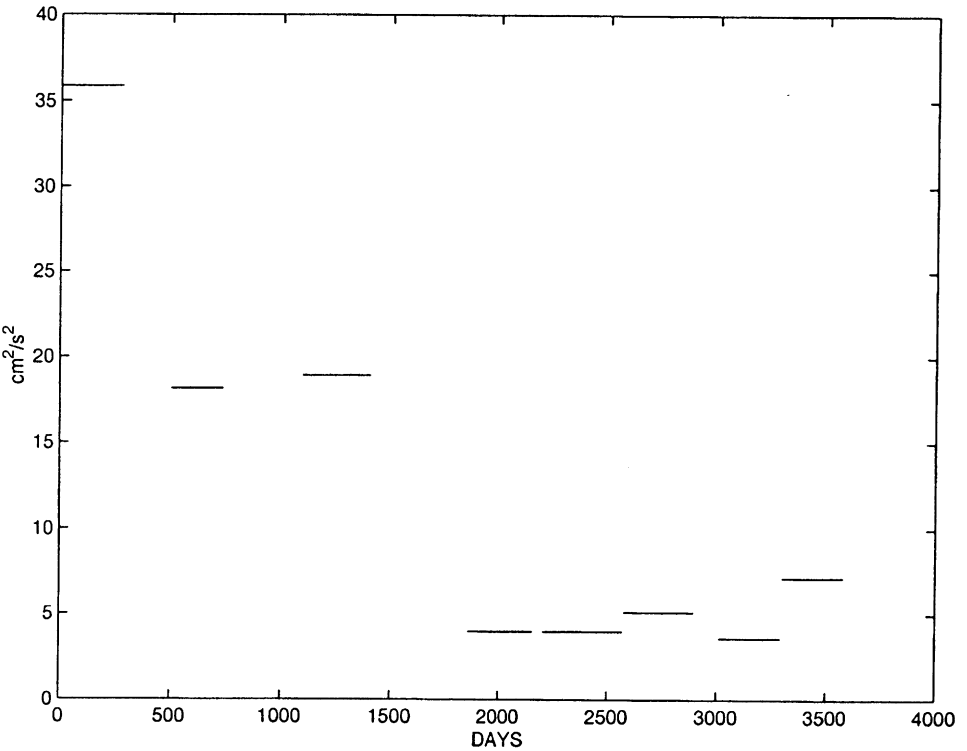

Fig. 4. Vertical average kinetic energy/unit mass/unit depth from Kiel's NEADS site mooring in the eastern North Atlantic (33°N, 22°W). The first record begins on 21 October 1980.

fluctuating forcing fields, much longer altimetric records are required to address this question definitively.

3. The annual cycle of variability

3.1. Altimetry

Because external atmospheric forcing fields (wind stress and buoyancy fluxes) are subject to a pronounced seasonal cycle over much of the globe, one can expect to gain insight into the ocean eddy and more general variability fields and their relationships to the forcing functions by focussing on the extent to which a seasonal cycle appears in the variability fields itself. On the global average, neither the frequency spectrum of γ nor that of γ^2 in Fig. 2, display more than the very slightest indication of any excess energy at the annual cycle. There appears to be no significant annual change in the global average velocity or energy level. Such a difference might have been expected because of the asymmetry across the equator of the oceanic area.

The regional story is different. A number of studies exist of apparent *circulation* changes on the annual cycle.[3] For example, from GEOS3 altimeter data, Fu et al. (1987) found a seasonally varying Gulf Stream transport down-stream of Cape Hatteras with a maximum around April, and a minimum in December, lagging the local wind stress variations by 2–3 months (see also Zlotnicki, 1991; Kelly, 1991). From GEOSAT data, Shum et al. (1990) found variations in mesoscale eddy energy of about 300 cm^2/s^2 in the Gulf Stream area, which they related to the lateral shift of its axis with seasons. Similar variations where reported by Tai and White (1990) from the Kuroshio region (25°–45°N, 140°–170°E) where they found a minimum in sea surface height variability during winter and a subsequent steady increase until fall. Based on GEOSAT and T/P data, White Heywood (1995) found seasonally varying eddy kinetic energy over large parts of the subpolar gyre of the North Atlantic – which they relate to similar changes in wind forcing.

To focus on the annual cycle in variability energy, the seasonal anomalies in K_S are shown in Fig. 5 as they emerge from the full four year period. Their percentage relative to the mean K_S is displayed in Fig. 6. Seasons are defined as in Stammer and Wunsch (1994) over three-month periods with spring starting in March. These figures show a complex geographical pattern. In the northern hemisphere, the largest amplitudes occur during winter and spring in the north-eastern areas of the Pacific and Atlantic, and along the North Equatorial Current; the western subtropical gyres and the North Equatorial Counter Current are more energetic during summer and fall.

For a more quantitative description, Fig. 7a shows the same seasonal change in eddy energy, but zonally averaged between 25° and 35°W in the Atlantic Ocean. North of 35°N there is enhanced energy present during the winter/spring, while the summer/fall period is low in energy. The opposite is true for the tropics where summer and fall are characterized by high eddy activity, possibly associated with the instability of the North Equatorial Counter Current (NECC) at about 10°N during its maximum strength. Note that a pronounced semi-annual variation is found in the sub-tropics between 20°N and 35°N, where both spring and fall are characterized by enhanced energy, while summer and winter have low variability. The southern hemisphere shows generally less variation in eddy energy. The most conspicuous features in the South Atlantic are the energy peak around 20°S during spring and at around 50°S during fall. In terms of percentage (Fig. 7b), the largest variations appear in low latitudes with up to 70% variations in K_S at the equator. The northern hemisphere stays below 20% change, mostly below 10% of K_S, and the southern hemisphere shows variations no bigger than about 5% of the mean.

Results from the central Pacific (180°–190°E) are displayed in Fig. 7c and d, respectively. (The detailed structures in the tropical amplitudes depend on the

[3] A chart of the annual cycle of the seasurface height itself (as opposed to the square of its slope), may be seen, e.g., in Wunsch and Stammer (1998). The largest signals of those primarily surface-heat flux driven changes are in the western boundary currents. Discussion of the annual cycle in the circulation, including apparent annual period baroclinic waves (e.g. Chelton and Schlax, 1996) is beyond our present scope, however.

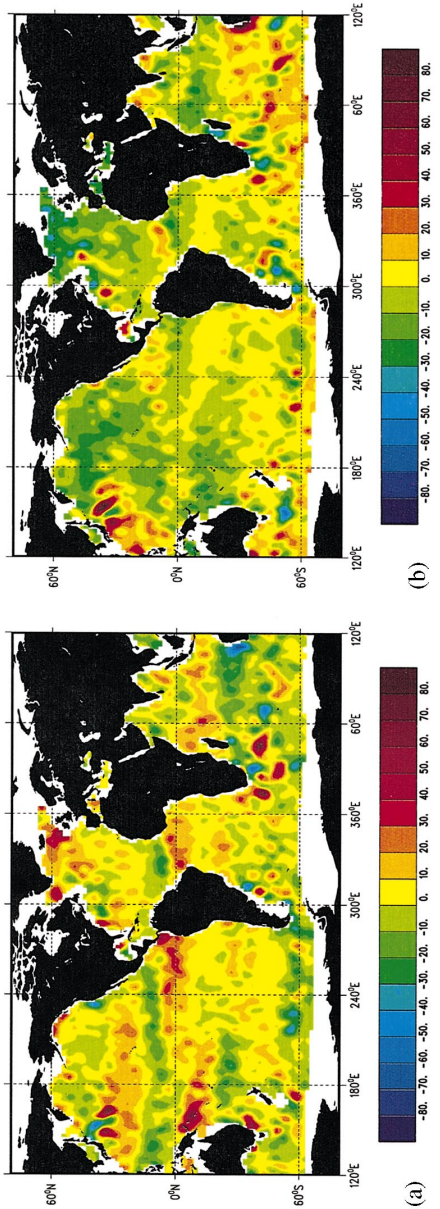

Fig. 5. Seasonal K_S anomalies estimated from the 4 yr of T/P data: (a) MAM, (b) JJA, (c) SON, (d) DJF. Units are cm^2/s^2.

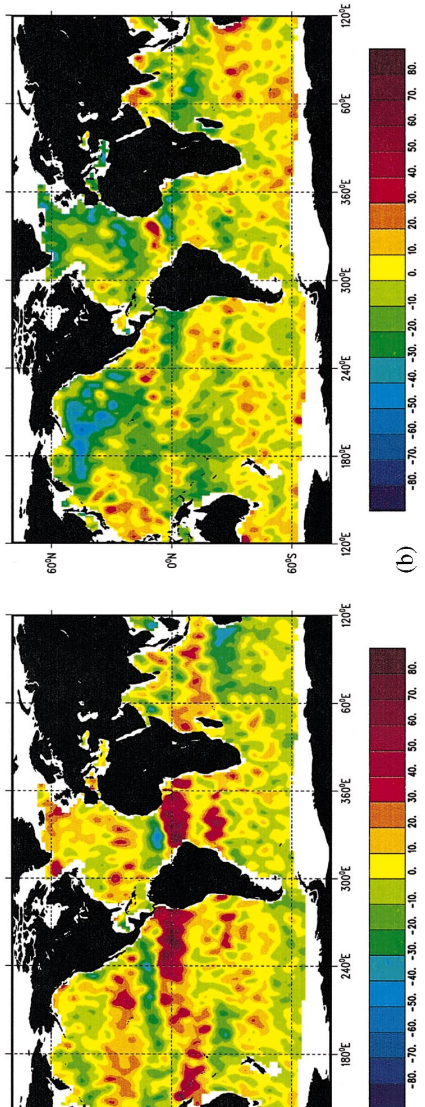

Fig. 6. Seasonal anomaly percentage of the mean for the K_S anomalies estimated from the 4 years of T/P data: (a) March–April–May, (b) June–July–August, (c) September–October–November, (d) December–January–February.

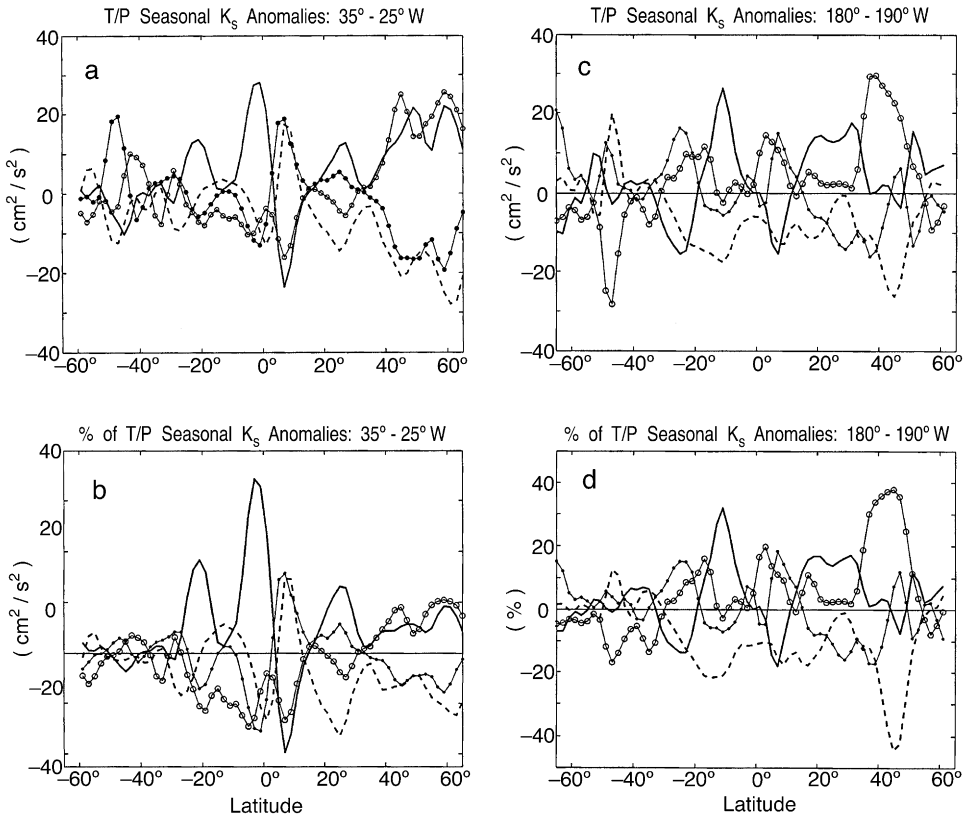

Fig. 7. Zonal averages of seasonal K_S anomalies and their percentage with respect to the total field, respectively, as they result from zonal averaging between 20° and 30°W in the Atlantic Ocean, and 180° and 190°E in the Pacific. Lines represent spring (solid), summer (dashed), fall (solid with solid dot), and winter (solid with open dots).

location of the meridional section with more energy to the east of 190°E; see Figs. 5 and 6.) Along this section, the biggest variations occur around 40°–50°N, where changes are up to 40% of the total energy, with a maximum and minimum present in winter and summer, respectively. Overall, the percentage change is higher in the Pacific than in the Atlantic, and seasonal changes in K_S are more complex.

To focus on the purely seasonal signal present in K_S, we estimated the amplitude and phase of an annual harmonic, which is least-squares fit to 4 yr worth of monthly K_S estimates. Because the seasonal cycle is not a purely periodic phenomenon, this description is only a partial one. As an example, Fig. 8 shows the actual anomaly of kinetic energy at the location 30°W, 55°N and the fit of an annual harmonic superimposed on a trend of about 10 cm^2/s^2 per year (solid line). The dashed line includes, in addition, the semi-annual harmonic. The amplitude of the annual harmonic is 29 cm^2/s^2 superimposed on a mean of 113 cm^2/s^2. It is apparent that each

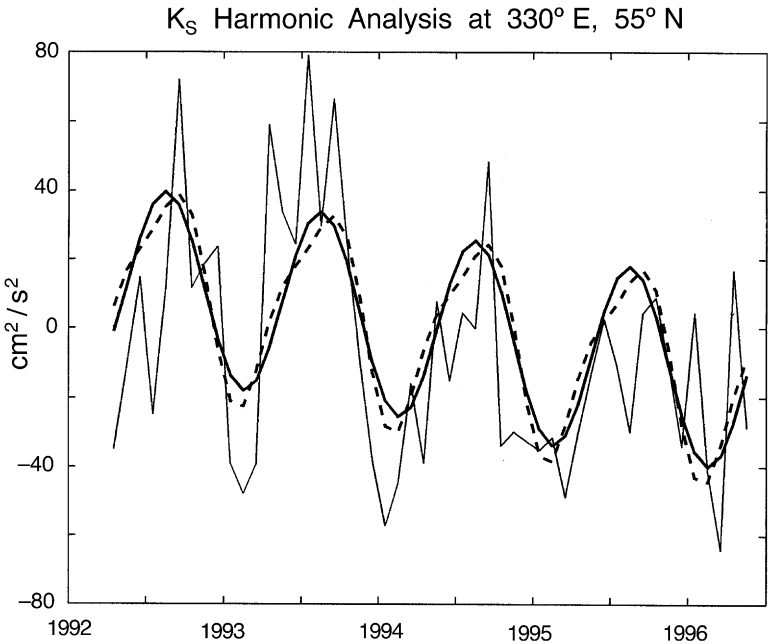

Fig. 8. Anomaly of K_S at 30°W, 55°N from the altimetric slope (dotted). A slow interannual drift is visible. The solid curve is the fit of the annual harmonic superimposed on a trend and the dash-dot curve includes the semi-annual fits in addition. The mean value at this location is 113 cm^2/s^2.

year is different in the data, and the changes are more complex than any single sinusoid can describe.[4]

The geographical distribution of the amplitude and the phase of the annual harmonic are shown in Fig. 9a and 9b, respectively. Maximum amplitudes of up to 200 cm^2/s^2 are located along major western boundary currents and along the Antarctic Circumpolar Current (ACC). Enhanced amplitudes cover the area of the NECC in the Pacific and Atlantic, but especially the northeastern North Atlantic and the Labrador Sea. Note also the local maximum at the location of the Great Whirl in the Indian Ocean, which occurs around September as observed previously (Swallow et al., 1983). Most of the seasonal variations in K_S are below 15% of the amplitude of the pure seasonal harmonic (Fig. 9c). This result is especially true for the southern hemisphere, and for the subtropical gyres and western boundary currents in the North Pacific and North Atlantic Oceans. At a few locations, however, seasonal K_S variations are substantial. Those regions showing 30–40% changes relative to the mean are primarily confined to the eastern North Pacific, the subpolar gyre and the eastern

[4] The small contribution by the semi-annual energy suggests little contribution by aliases from residual K_1 tides.

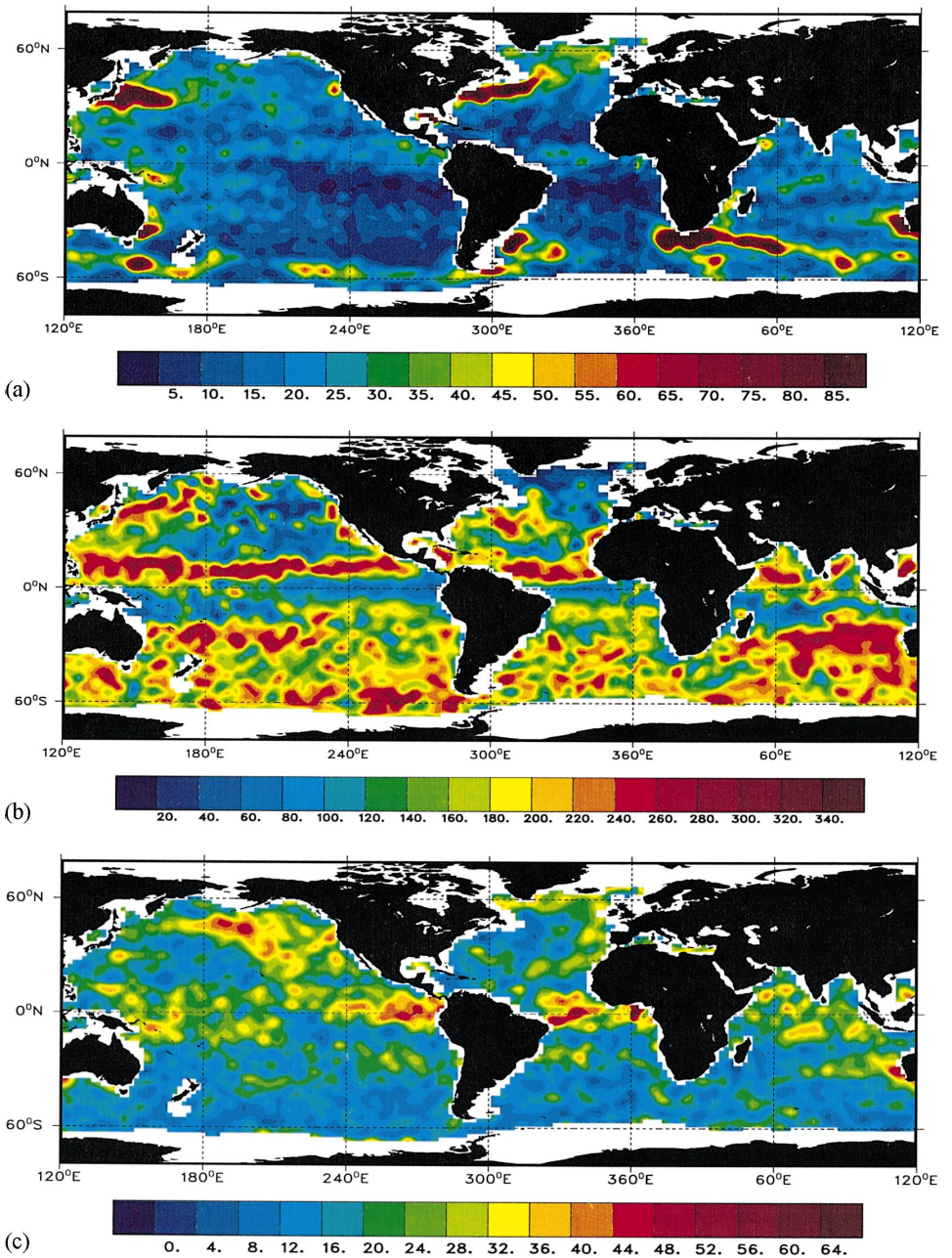

Fig. 9. The seasonal cycle of K_S estimated from monthly K_S fields. Shown are (a) the amplitude in cm^2/s^2, (b) the phase in degrees relative to 1 January, and (c) the percentage the amplitude is of the mean variability.

boundary of the North Atlantic, the tropical oceans, as well as a region west of Australia in the Indian Ocean.

Insight into physical mechanisms leading to the observed seasonal changes in K_S can follow from the phase of its annual cycle and its relation to forcing functions. The phase field in Fig. 9b shows a complex structure, especially in the northern hemisphere, but much of the structure coincides with the major current systems. Focusing on the northern hemisphere Atlantic and Pacific, there are a number of features conspicuous in Fig. 9b:

1. North Equatorial Counter Current (NECC). Here one sees up to 30% variation of the kinetic energy on the annual cycle. A maximum occurs in summer/fall along with the maximum strength of the NECC, i.e., when its instability waves are most prominent (e.g., Philander, 1990; McPhaden, 1996).
2. North Equatorial Current (NEC): A maximum occurs in spring, although changes in energy levels on the annual cycle are marginal here.
3. Boundary current extensions: The western subtropical gyres show the largest variations of energy on the annual cycle, with the maximum amplitude occurring in late summer/early fall in both oceans.
4. Eastern basins: Wintertime maximum energy occurs in the central Pacific and eastern Atlantic along with those in the NEC.
5. Eastern boundary: In both the Atlantic and the Pacific, the eastern boundary shows enhanced energy in summer/fall. For the Pacific this maximum coincides with maximum strength of the California current and the associated shear-instabilities (see, e.g., Strub et al., 1987).
6. Subpolar gyres: The maximum in the Labrador Sea occurs in April after wintertime convection has taken place and which hypothetically gives rise to strong baroclinic instability and associated eddy variability. In contrast, the more eastern portions show a maximum a few month earlier and more in phase with the wind stress curl maximum over those locations as discussed below. This phase shift in K_S is present more dramatically in the North Pacific, where the western basin is out of phase with the eastern basin by about six months.

3.2. Current meter results

We now describe the annual cycle as observed in the moorings insofar as it is possible (the reader is reminded that these moorings are distributed over about 20 yr in time and the interannual variability described above must be kept in mind). Before doing so, we note that a few existing studies have addressed the question previously using both current meters and surface drifters.

3.2.1. North Atlantic

A seasonal signal in eddy kinetic energy levels was reported by Dickson et al. (1982) to be present in current meter records from a number of sites east of 20°W in the northeastern North Atlantic. They interpreted their results as supporting the local wind-forcing hypothesis in the interior oceans. However, neither they nor Müller and

Siedler (1992) detected any significant seasonal variation in current meter records from the eastern North Atlantic further south. In contrast, Klein and Siedler (1989) saw a seasonal variation in the Azores Current showing a more narrow stream during the summer months and a simultaneously enhanced eddy activity.

Using surface drifters, Richardson (1983) analyzed seasonal variations in K_E for near-surface conditions. He found a seasonally varying eddy energy in the North Atlantic Current (NAC) region 40°N–54°N, 10°W–38°W with a maximum in eddy kinetic energy during spring (May/June) about 4 months after the maximum in the wind stress and a minimum in autumn (August/September). Along the eastern Gulf Stream (38°N–42°N, 45°W–52°W), he found a minimum in July/August and maximum in autumn/spring, Brügge (1995) reports maximum variability along the NAC (at 30°W) in winter and a minimum in fall, while along the Azores current he finds a maximum in fall.

One expects the current meter moorings to exhibit somewhat different results than the altimeter does. The moorings are best used for estimating the water

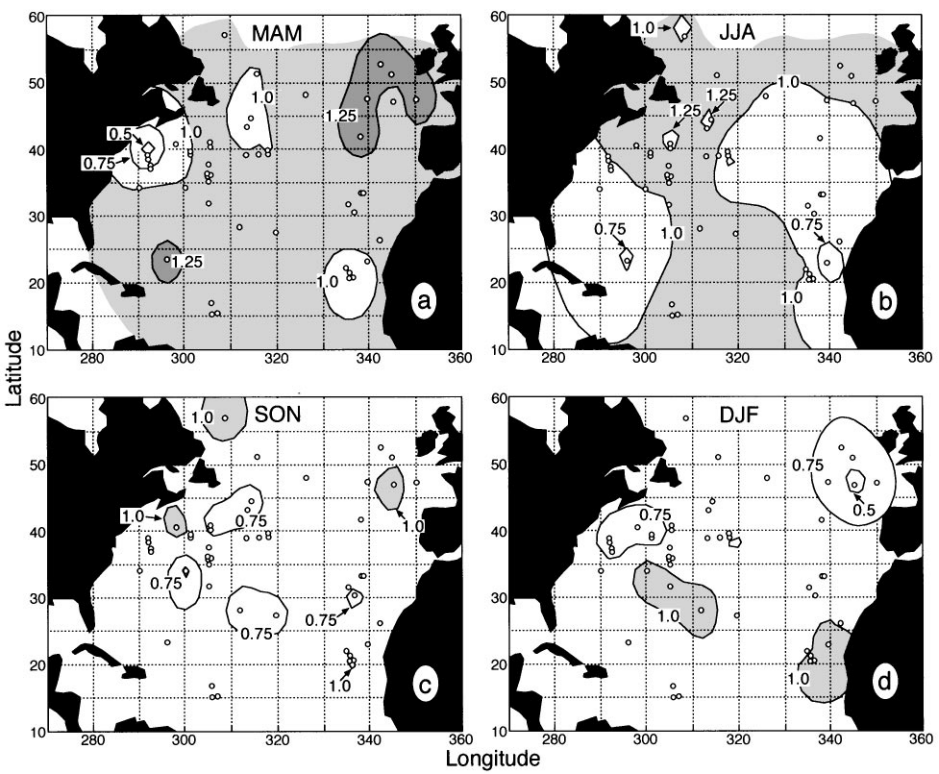

Fig. 10. Seasonal anomalies of the North Atlantic surface kinetic energy as depicted in the current meter records, for (a) spring (March–April–May), (b) summer (June–July–August), (c) fall (September–October–November), and winter (December–January–February). These are the ratios of the seasonal anomalies to the apparent annual means of each record. (c)–(h) Similar fields, but from TOPEX/POSEIDON altimetry redrawn from Fig. 6.

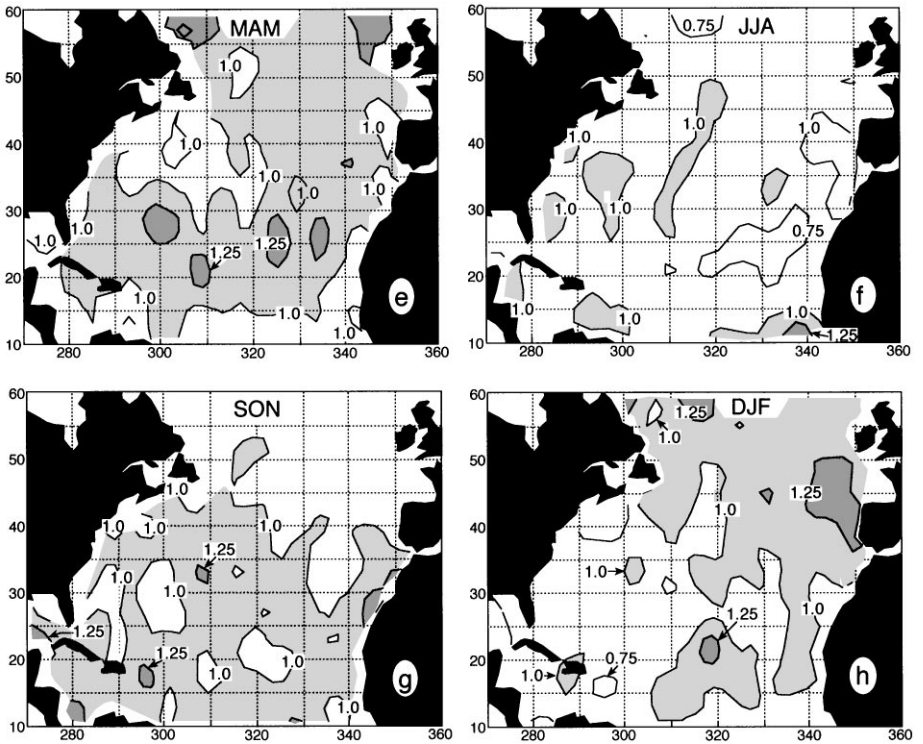

Fig. 10. Continued.

column-averaged kinetic energy, while the altimeter directly measures the seasurface kinetic energy. To obtain the latter from the moorings requires an extrapolation of the modes to the surface. Fig. 10a–d displays the seasonal changes in surface kinetic energy in the North Atlantic as computed on the moorings through extrapolation. The definition is the so-called $T^{(1)}(0)$ described in Wunsch (1997), which permits the modes to be phase-locked. The altimetric results from Fig. 7 are redrawn here on the same scale for comparison (Fig. 10e–h). The results are depicted as the spring (March–April–May), summer (June–July–August), etc. fractions of the yearly average kinetic energy. Few moorings actually span a full year and few if any isolated moorings by themselves produce significant values; therefore the yearly averages, against which anomalies are measured, are very uncertain. (The maps were created by an objective – but not optimal – algorithm that arbitrarily set a white-noise level to 10% of the signal value at each mooring, and used a 500 km correlation scale). Results are credible whenever large scale patterns emerge from several moorings.

Only in the northeast corner of the North Atlantic and in the Gulf Stream recirculation system is there an indication from the current meters of a seasonally varying eddy kinetic energy, with a winter minimum present in surface kinetic energy in both locations. In spring, the northeastern region is above the annual average while

the near-Gulf Stream region appears to display peak energy in mid-summer. There is little evidence of an annual cycle elsewhere, with some suggestion from the moorings that the interior North Atlantic has low energy during the autumn.

One can compare these current meter results to the altimetric values with all the caveats already stated. According to Fig. 9b, the northeast North Atlantic reaches a maximum in altimetric K_S in April, which is consistent with the current meter result. Gulf Stream variability appears to reach a maximum value in June to early autumn, which is at least crudely consistent with the zero-order interpretation of the altimetry. Elsewhere in the North Atlantic interior, both current meters and altimetry are consistent with a very weak annual cycle.

There tends to be better agreement between the mooring data and the sinusoidal annual cycle fit to the altimetry than there is with the four-season anomalies. One rationalization is that the sinusoids represent the temporally stable elements of the annual cycle, with the full anomalies containing stochastic elements which shift radically from year-to-year.

3.2.2. North Pacific

The Pacific moorings are confined to a narrow latitude band between about 30° and 42°N. At most a 25% variability with season is visible (Fig. 11), with a tendency for the eastern Pacific to have a maximum surface kinetic energy in winter and a minimum in autumn, with the western part of the ocean being high in the summer and a minimum in winter as in the near-Gulf Stream region. Overall, this quantitatively confirms the altimetric results (Fig. 9).

3.2.3. Current meter modal decomposition

The temporal variability also can be described approximately in terms of its modal content – keeping in mind (Wunsch, 1997) that in many places there is significant mode-coupling in time. Figs. 12 and 13 depict the North Atlantic seasonal fractions broken down by the barotropic (mode-0) and first baroclinic mode (mode-1). Note that these values describe the water column average kinetic energy, not the surface kinetic energy. (Wunsch (1997) shows the distribution of the water column mean kinetic energy – a quantity which is independent of any mode coupling). The low values of surface kinetic energy in the northeastern North Atlantic during winter coincide with reductions in energy of both mode-0, and mode-1, but particularly in the former. The spring maximum there is dominated by high energy in the first baroclinic mode.[5] The near-Gulf Stream region also shows a somewhat stronger barotropic contribution to the seasonal cycle overall – in part consistent with the extremely high barotropic energy found in this region relative to the rest of the ocean. (See Wunsch (1997) for charts of the percentage contributions of the different modes to the time-mean sea surface kinetic energy.)

[5] A significant compilation in these results, which we have not addressed here however, arises in high-latitude regions where the seasonal change in stratification is so large that the annual mean modal decomposition breaks down as an adequate representation – see the example in Wunsch (1997).

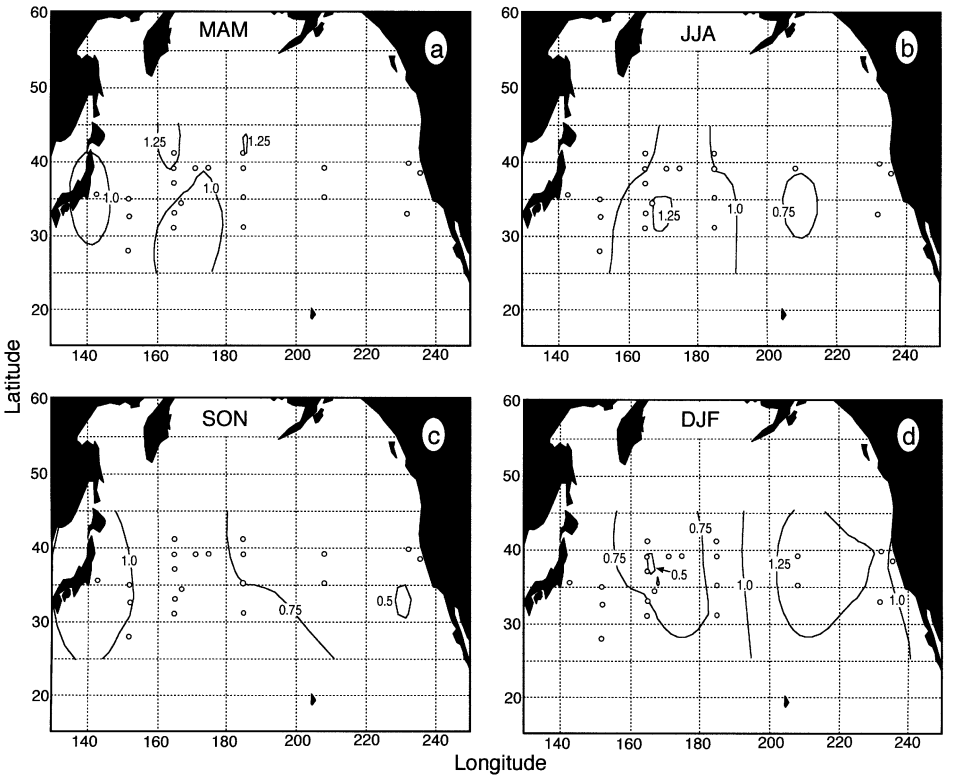

Fig. 11. Same as Fig. 10a–d, except for the North Pacific current meter records.

In the Pacific eastern basin (not shown), both modes appear to have more energy in winter with a low in summer, consistent with the previous results of Koblinsky et al. (1989). The western side of the ocean is 180° out of phase with this behavior.

Current-meter moorings and altimetry thus both consistently produce a 25% maximum seasonal change in the surface kinetic energy. The barotropic and first baroclinic modes dominate the vertical average kinetic energy, and both modes contribute to this seasonal cycling of the surface kinetic energy in a pattern which varies with position. While a wind-induced barotropic variability of O (1 $cm^2 s^{-2}$) can represent a significant fraction of the total eddy kinetic energy in the deep ocean, especially in the mesoscale-deficient eastern basins in the northern Pacific, it is of minor importance for the upper layers.

4. Relation to wind forcing

We now turn to the question of how much of the variability – both interannual, and on the annual cycle – is likely to be a direct consequence of fluctuations in the *local*

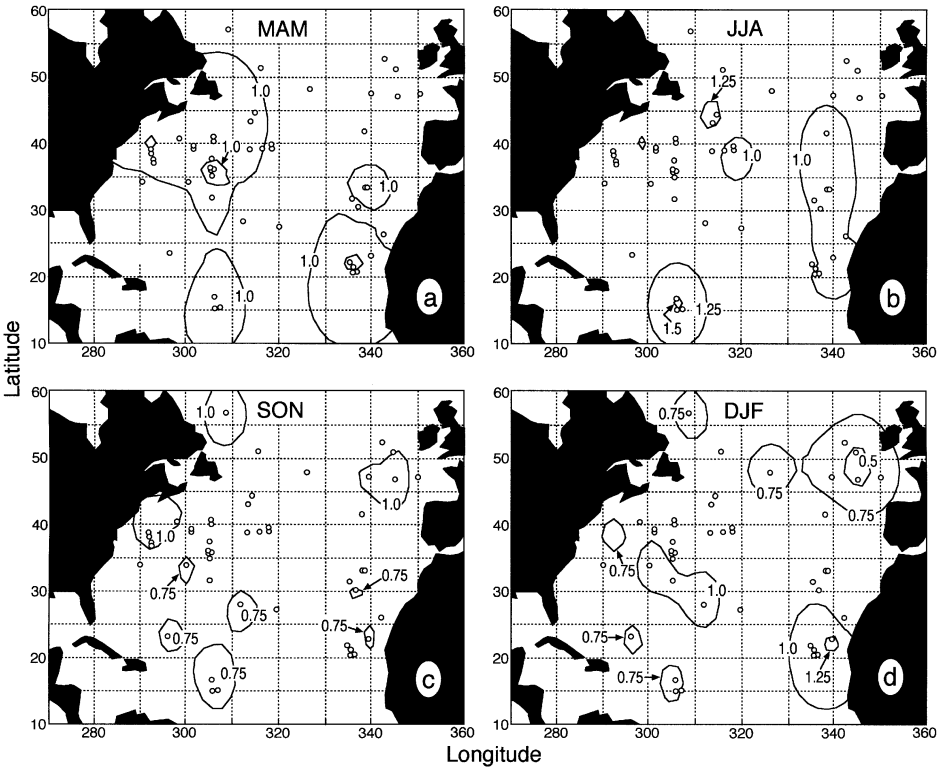

Fig. 12. Fraction of the water column average kinetic energy in the North Atlantic barotropic mode by season.

wind field forcing? If the wind field exhibits similar spatial and temporal patterns of change as does the ocean mesoscale variability, one has at least an indication of a cause-and-effect relationship.

4.1. Interannual variation of the wind field

Fig. 14 shows the equivalent of Fig. 1b but for the National Center for Environmental Prediction (NCEP) wind stress square $\tau^2 = \tau_x^2 + \tau_y^2$ (Fig. 14a and b), and $curl(\tau)^2$ (Fig. 14c and d), displaying the differences, year-four minus year-one of the T/P mission in both their mean and their standard deviation, respectively. The τ^2 fields show an intriguing similarity to observed changes in K_S, especially in the Atlantic, north of 50°N, where the atmospheric fields indicate a decrease of the mean and the standard deviation of τ^2. South of 50°N, the opposite is true, with both fields increasing. Those changes suggest a shift of the mean westerlies equatorward by about 10° to 20° to about 40°N. At the same time, the variability associated with the storm systems changes in much the same way, in a pattern connected to the North Atlantic Oscillation (NAO). In the Pacific, similar but less dramatic changes are observed,

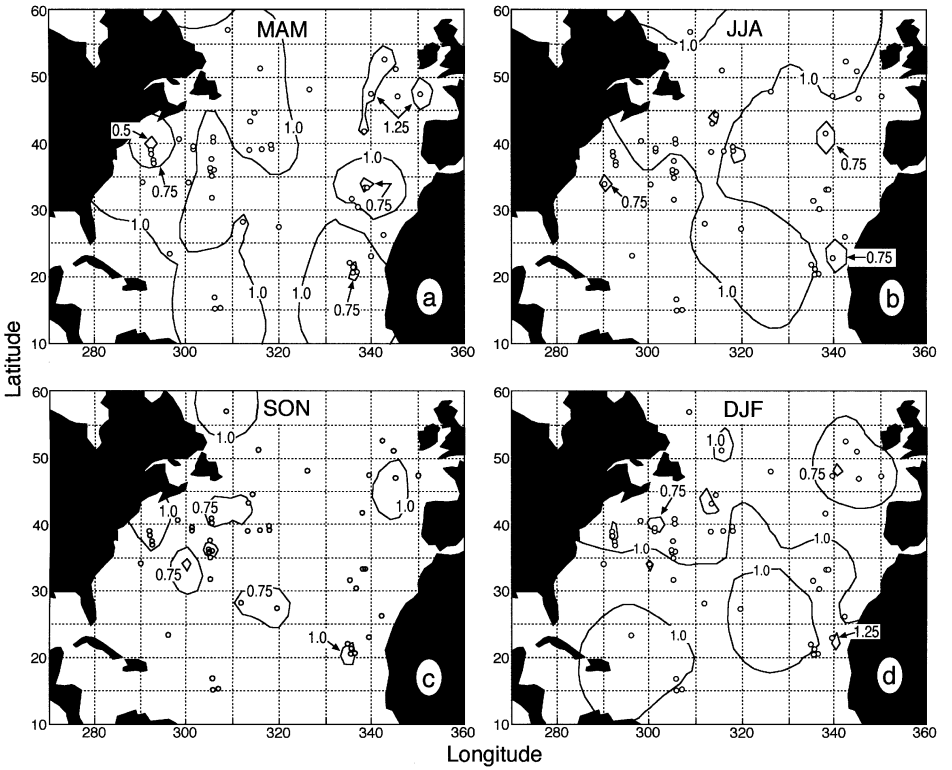

Fig. 13. Same as Fig. 12, except for the first baroclinic mode.

although the Trade Winds seems to have increased more than in the subtropical Atlantic.

Changes observed in Fig. 1b could therefore be induced by a changing mean ocean circulation and the associated shifts in the oceanic variability pattern. Changes in K_S could likewise be associated with the shift in atmospheric storm pattern and the associated direct energy input by the wind fields. The former correspondence would be consistent with the mean sea surface height in the subtropics, which indicates a strengthening of the subtropical gyres and western boundary currents from the first to the fourth year of the T/P mission (Fig. 15). The latter can especially be anticipated to be true in high latitudes where the wind field has highest energy.

4.2. Annual cycle of the wind field

To illustrate the extent to which changes in the wind fields are consistent with those in K_S, Fig. 16 compares timeseries of monthly K_S estimates with monthly averages of τ^2 (Fig. 16a) and curl$(\tau)^2$ (Fig. 16b), all averaged over regions spanning 10° on a side.

Variations of K_S on the annual period are correlated with both τ^2 and curl$(\tau)^2$ in the northern part of the Atlantic. Highest correlations (up to 0.7, but there are not many degrees of freedom) are found east to Cape Farewell, where K_S is almost in phase with the atmosphere. Further east, and especially in the Labrador Sea, an increased oceanic phase lag of up to three months is observed. In the subtropics and tropics, atmospheric energy is substantially reduced, and correlations, which are marginal at best, indicate changes in K_S and the atmosphere to be out of phase in the western subtropical gyre on the annual period.

It is noteworthy that the interannual changes in τ^2 and curl$(\tau)^2$ present in high latitudes are clearly reflected in the amplitudes of K_S: in particular variations in the peak amplitudes of τ^2 are strikingly similar to winter time K_S maxima, which show

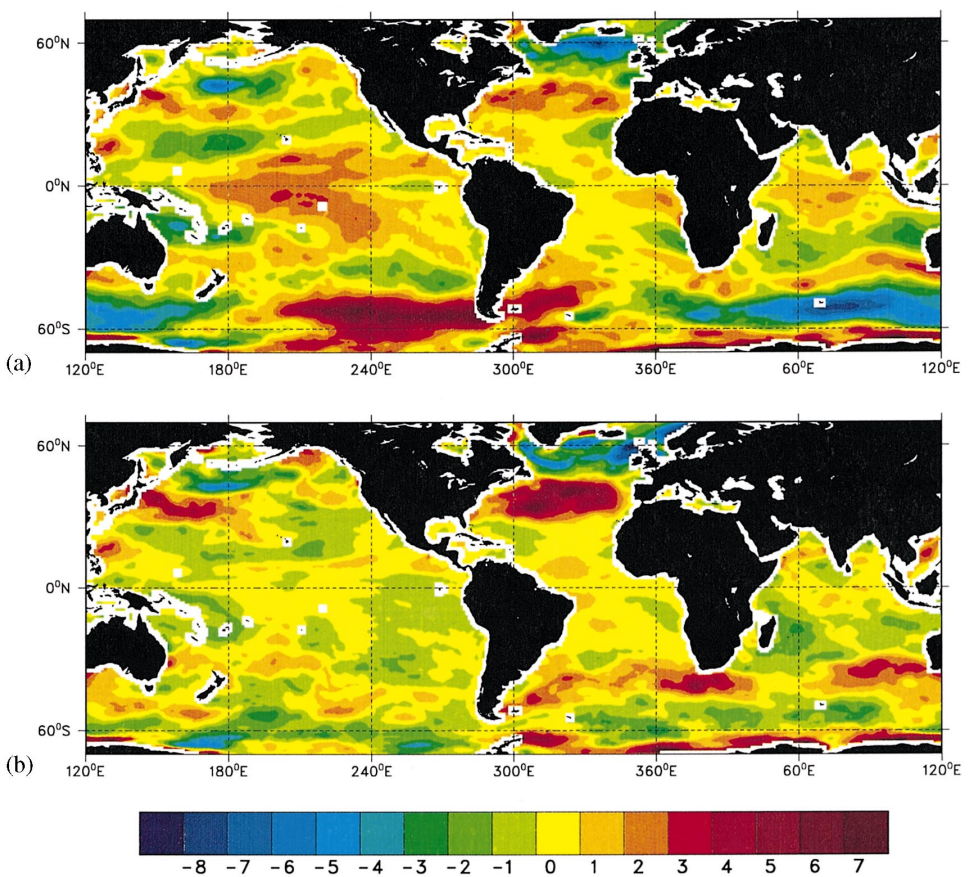

Fig. 14. Difference in (a) mean and (b) standard deviation of the wind stress magnitude $|\tau|$ estimated individually over the fourth and first year of the T/P mission from NCEP fields. (c) and (d) show similar fields but from curl(τ). Units are N/m^2 in (a) and (b) and 10^{-8} N/m^3 in (c) and (d).

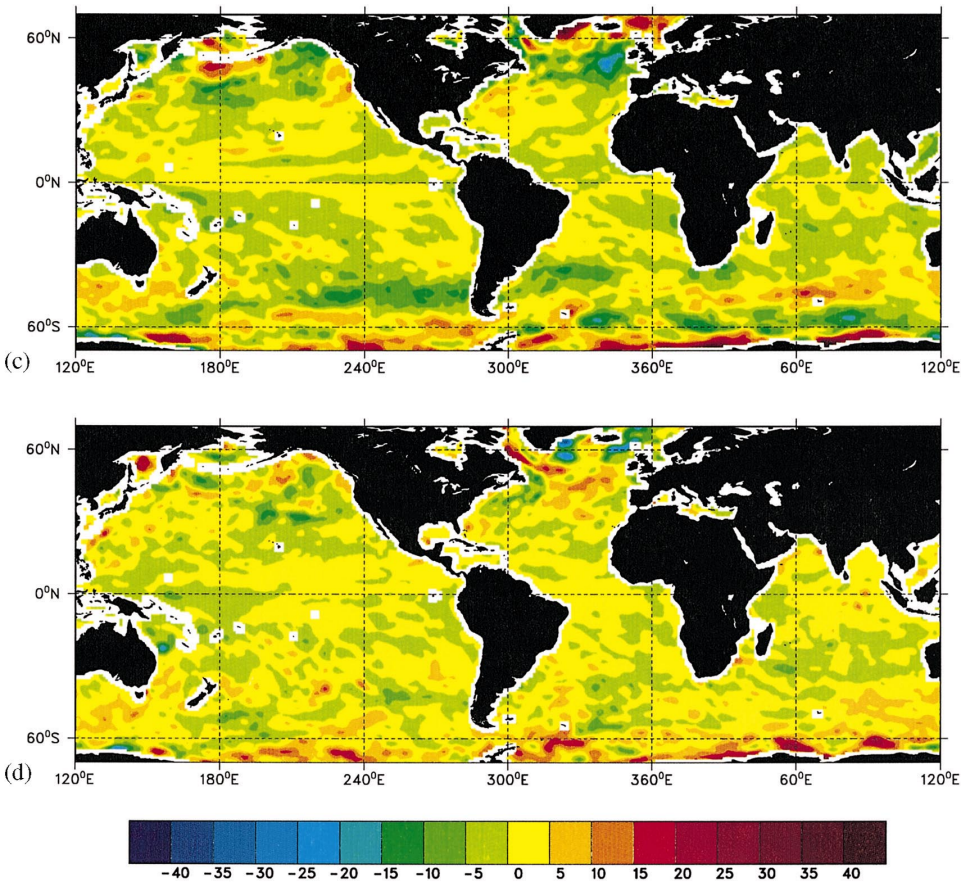

Fig. 14. Continued.

a steady decline in eddy variability over the subpolar North Atlantic during the entire T/P period.

Fig. 17 displays the annual cycle amplitudes and phases of τ^2 and curl$(\tau)^2$. There is no obvious relationship between the seasonal changes present in the forcing fields and the regions of most intense seasonal changes in eddy energy variability – except in the locations discussed above. Instead, much of the mid- and low-latitude structure visible in Fig. 9 appears to arise from the patterns of the oceanic mass circulation. This circulation is largely a consequence of the wind stress field, but only as the solution of a complex initial/boundary value problem which produces scales in the ocean response radically changed from those present in the atmospheric forcing. Thus there is usually no simple relationship between the purely local wind field and the eddy energy – despite the attractive simplicity of that hypothesis.

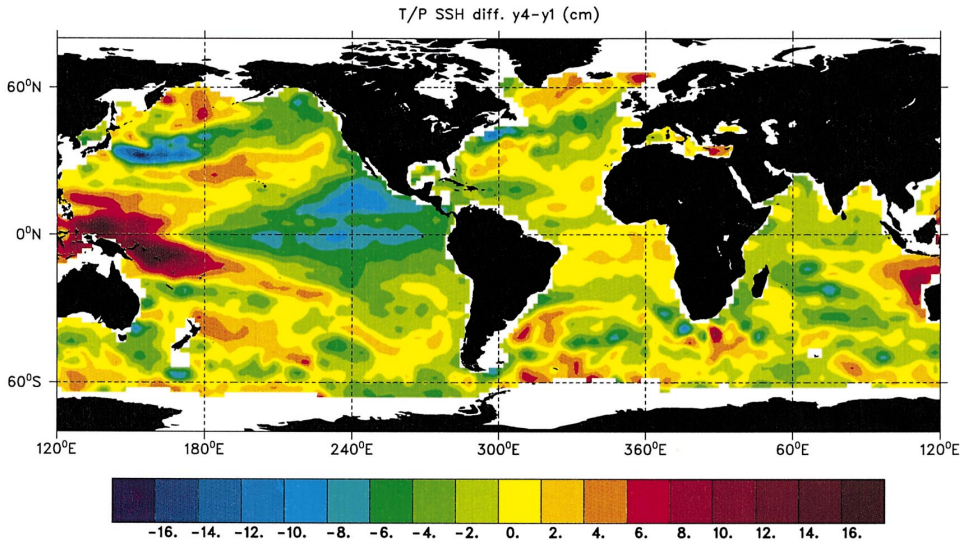

Fig. 15. Difference in mean SSH estimated from year 4 minus year 1 of the T/P mission. Contour interval is 2 cms.

5. Summary and concluding remarks

On a global average, there is no evidence for any trends in variability energy over the 4-yr altimetric record, and no evidence for a global average seasonal cycle. On a regional basis, however, an intricate pattern emerges both in 4-yr trends, and in the amplitude and phase of the annual cycle of altimetric variability energy. Most of this pattern in mid- and low-latitude oceans is related to the intense currents of the general circulation, with no obvious direct connection to annual changes in the wind field. Current-meter results indicate that barotropic and first baroclinic modes dominate the vertical-average kinetic energy, and both modes contribute to this seasonal cycling of the surface kinetic energy in a pattern which varies with position. A wind-induced barotropic variability of $O(1\ cm^2\ s^{-2})$ is a significant fraction of the total eddy kinetic energy in the deep ocean, especially in the mesoscale-deficient eastern basins in the northern Pacific.

In most regions, the eddy source terms are associated with the ocean flow field (baroclinic and barotropic instability) and most of the seasonal and secular changes of the eddy energy variability are associated with similar fluctuations in the strength and stability properties of these currents, and in the strength of the interactions with local bottom topography. Exceptions are a few places with high wind energy, notably in the North Pacific and in the northern North Atlantic, where a significant correlation of altimetric eddy kinetic energy with the NCEP wind stress fields can be found both on annual and interannual time scale.

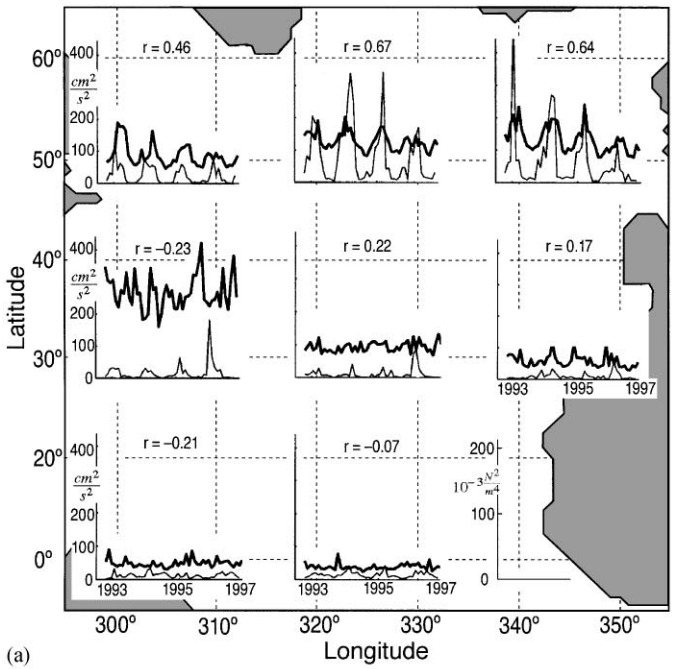

(a)

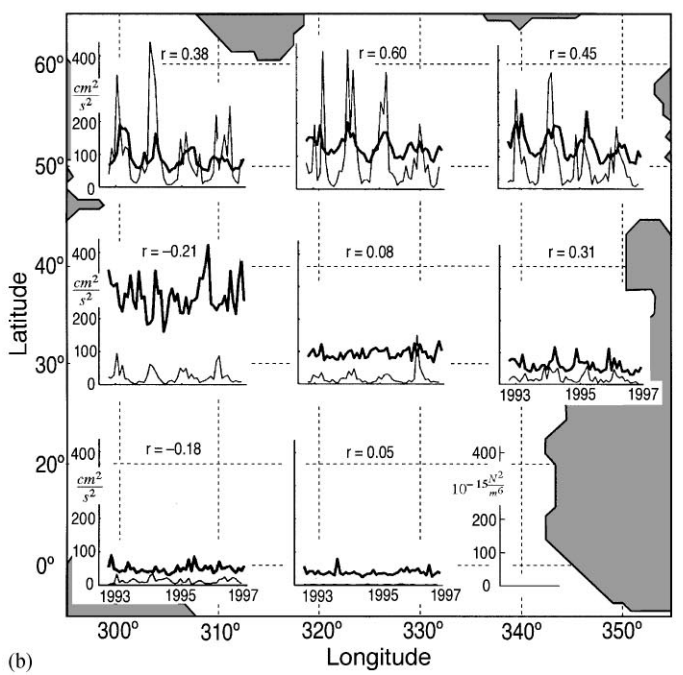

(b)

Fig. 16. (a) Timeseries of monthly K_S (bold lines) and τ^2 (thin lines) estimated in various regions spanning 10° on a side in the North Atlantic. The correlation coefficient r between the curves is also provided. (b) Similar to Fig. 16a, but for curl$(\tau)^2$, instead of τ^2.

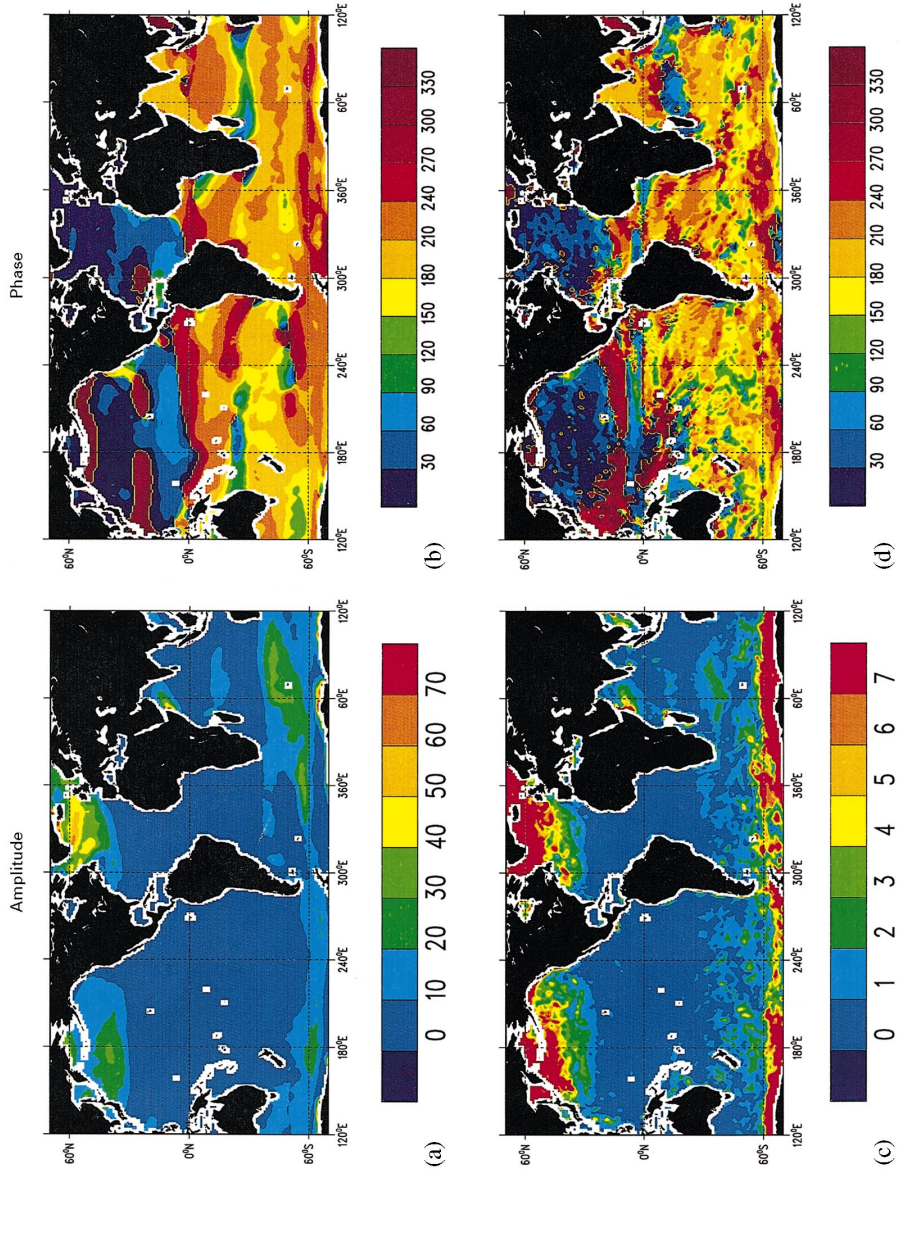

Fig. 17. Annual cycle of atmospheric forcing fields. Shown are the amplitudes and phases for (a, c) τ^2, and (b, d) curl$(\tau)^2$, respectively. Units are (a) $(N/m^2)^2$ and (b) 10^{-15} $(N/m^3)^2$.

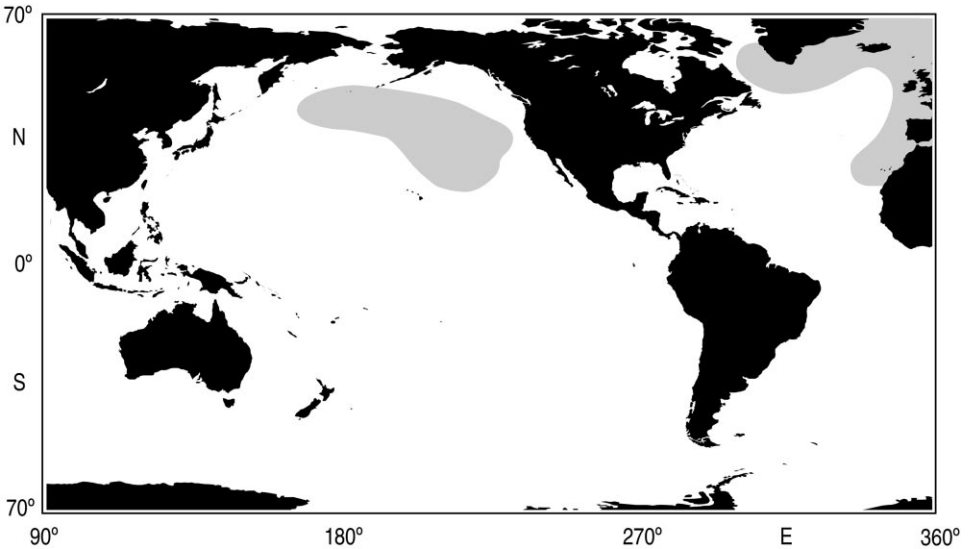

Fig. 18. Schematic diagram indicating those regions where a significant contribution of the wind field to the observed eddy energy was found in this analysis.

A clear indication of the direct impact of the wind on the ocean eddy field is obtained here from locations situated in the high wind-energy regions of the north Pacific and subpolar North Atlantic. In those regions (Fig. 18), observed variations in eddy kinetic energy on seasonal and interannual periods are significantly correlated with similar changes in wind stress. The figure is based on various criteria, including a significant fraction of K_S variability on the annual cycle, a significant amplitude of the annual harmonic in the atmospheric fields and a phase difference between K_S and $\mathrm{curl}(\tau)^2$ not exceeding 90° with the atmosphere leading the ocean. Note that the figure is consistent with the results of Fu and Davidson (1995) who found significant indications of a barotropic response of the ocean to time-dependent wind forcing in about the same region of the Pacific as identified here. The locations in the Atlantic, where similar results are seen, were outside their study region. In interpreting Fig. 18, however, it should be kept in mind that the southern hemisphere exhibits only marginal seasonal changes in its wind stress.

The conclusions drawn by Dickson et al. (1982) – that the wind is responsible for most of the observed eddy variability remote from boundary currents – are not consistent with present results. Instead a direct wind impact seems to be limited to very high latitudes, and even there only some fraction of the observed eddy energy is directly related to wind stress. Few other simple generalizations appear to be globally applicable; a fuller description requires a series of regional dynamical studies.

Obvious physical mechanisms that need to be explored for a full explanation of observed changes in eddy energy include an annual fluctuation in the degree of barotropic and baroclinic instabilities, and in the strength of the interaction with

particular topographic features as the circulation strength varies under varying wind and buoyancy forces. A discussion employing a model framework will be published elsewhere. Here, in keeping with our primarily descriptive intentions, we have simply called attention to some of the major elements related to the surface wind stress.

We conclude that although a refined a rigorous test has not been employed, there is some (possibly marginal) evidence of true secular changes in regional kinetic energy from 4 yr of altimetry. In the light of present results it seems likely that the eastern North Atlantic exhibits secular changes over 5–10 yr in eddy energy by about 100% and more as seen by Müller and Siedler (1992) at the NEADS mooring site. Those changes are not directly related to local wind forcing. Neither the NCEP wind stress amplitude nor its curl near the NEADS location shows any significant correlation with the observed changes in eddy energy during the 1980s. The Müller and Siedler (1992) results therefore are a manifestation of the complex response of the ocean to local and remote forcing.

Acknowledgements

This work was supported in part by Contract 958125 with the Jet Propulsion Laboratory, and Grant NAGW-918 with the National Aeronautics and Space Administration. Contribution to the World Ocean Circulation Experiment (WOCE).

References

Beckmann, A., Böning, C.W., Brügge, B., Stammer, D., 1994. Eddy variability in the Central North Atlantic Ocean: results from surface drifters, satellite altimetry and numerical modeling. Journal of Geophysical Research 99, 20 381–20 392.

Brugge, B., 1995. Near-surface mean circulation and kinetic energy in the central North Atlantic from drifter data. Journal of Geophysical Research 100, 20 543–20 554.

Chelton, D., Schlax, M.G., 1996. Global observations of oceanic Rossby waves. Science 272, 234–238.

Dickson, R.R., 1989. Flow statistics from long-term current-meter moorings. The global data-set in January 1989. World Ocean Circulation Experiment. WCRP-30, WMO/TD – No. 337, 35pp. plus numerous tables World Climate Research Program.

Dickson, R.R., Gould, W.J., Gurbutt, P.A., Killworth, P.D., 1982. A seasonal signal in ocean currents to abyssal depths. Nature 295, 193–198.

Frankignoul, C., Müller, P., 1979. Quasi-geostrophic response of an infinite beta-plane ocean to stochastic forcing by the atmosphere. Journal of Physical Oceanography 9, 104–127.

Fu, L.-L., Keffer, T., Niiler, P., Wunsch, C., 1982. Observations of mesoscale variability in the western North Atlantic: A comparative study. Journal of Marine Research 40, 809–848.

Fu, L.-L., Davidson, R.A., 1995. A note on the barotropic response of sea level time-dependent wind forcing. Journal of Geophysical Research 100, 955–963.

Fu, L.-L., Smith, R.D., 1996. Global ocean circulation from satellite altimetery and high-resolution computer simulation. Bulletin of the American Meteorological Society 77, 2625–2636.

Fu, L.-L., Vazquez, J., Parke, M.E., 1987. Seasonal variability of the Gulf Stream from satellite altimetery. Journal of Geophysical Research 92, 749–754.

Gill, A.E., Green, J.S.A., Simmons, A.J., 1974. Energy partition in the large-scale ocean circulation and the production of mid-ocean eddies. Deep-Sea Research 21, 499–528.

Hogg, N.G., 1988. Stochastic wave radiation by the Gulf Stream. Journal of Physical Oceanography 18, 1687–1701.

Kelly, K.A., 1991. The meandering of the Gulf Stream as seen by the Geosat altimeter: surface transport, position and velocity variance from 73° to 46°W. Journal of Geophysical Research 96, 897–910.

Klein, B., Siedler, G., 1989. On the origin of the Azores Current. Journal of Geophysical Research 94, 6159–6168.

Koblinsky, C.J., Niiler, P.P., Schmitz, Jr., W.J., 1989. Observations of wind-forced deep ocean currents in the North Pacific. Journal of Geophysical Research 94, 10 773–10 790.

Large, W.G., Holland, W.R., Evans, J.C., 1991. Quasi-geostrophic ocean response to real wind forcing: the effects of temporal smoothing. Journal of Physical Oceanography 21, 998–1017.

Lippert, A., Müller, P., 1995. Direct atmospheric forcing of geostrophic eddies. Part II: coherence maps. Journal of Physical Oceanography 25, 106–121.

McPhaden, M.J., 1996. Monthly period oscillations in equatorial countercurrent. Journal of Geophysical Research 101, 6337–6359.

Mercier, H., Colin de Verdière, A., 1985. Space and time scales of mesoscales motions in the eastern North Atlantic. Journal of Physical Oceanography 15, 171–183.

MODE Group, 1978. The Mid-ocean dynamics experiment. Deep-Sea Research 25, 859–910.

Müller, P., Frankignoul, C., 1981. Direct atmospheric forcing of geostrophic eddies. Journal of Physical Oceanography 11, 287–308.

Müller, T.J., Siedler, G., 1992. Multi-year current time series in the eastern North Atlantic Ocean. Journal of Marine Research 50, 63–98.

Pedlosky, J., 1977. On the radiation of mesoscale energy in the mid-ocean. Deep-Sea Research 24, 591–600.

Philander, S.G.H., 1990. El Niño, La Niña, and the Southern Oscillation. Academic, San Diego, CA, 239pp.

Priestley, M.B., 1982. Spectral Analysis and Time Series. Vol. 1: Univariate Series. Volume 2: Multivariate Series, Prediction and Control. Academic, London, 890pp. plus appendices (combined edition).

Richardson, P.L., 1983. Eddy kinetic energy in the North Atlantic from surface drifters. Journal of Geophysical Research 88, 4355–4367.

Robinson, A.R. (Ed.), 1983. Eddies in Marine Science, Springer, Berlin, 609 pp.

Schmitz Jr., W.J., 1979. The MODE site revisited. Journal of Marine Research 47, 131–151.

Shum, C.K., Werner, R.A., Sandwell, D.T., Zhang, B.H., Nerem, R.S., Tapley, B.D., 1990. Variations of global mesoscale eddy energy observed from Geosat. Journal of Geophysical Research 95, 17 865–17 876.

Siedler, G., Zenk, W., Emery, W.J., 1985. Strong current events related to a subtropical front in the northeast Atlantic. Journal of Physical Oceanography 15, 885–897.

Stammer, D., 1997. Global characteristics of ocean variability from regional TOPEX/POSEIDON altimeter measurements. Journal of Physical Oceanography 27, 1743–1769.

Stammer, D., 1998. On eddy characteristics, eddy mixing and mean flow properties. Journal of Physical Oceanography, in press.

Stammer, D., Wunsch, C., 1994. Preliminary assessment of the accuracy and precision of TOPEX/POSEIDON altimeter data with respect to the large scale ocean circulation. Journal of Geophysical Research 99, 24,584–25,604.

Stammer, D., Böning, C.W., 1996. Generation and distribution of mesoscale eddies in the North Atlantic Ocean. In: Krauss, W. (Ed.), Warm Water Sphere of the North Atlantic Ocean. Gebrüder Bornträger, Berlin, 159–193.

Stammer, D., Böning, C.W., Dieterich, C., 1999. The role of variable wind forcing in generating eddy energy in the North Atlantic, to be submitted for publication.

Strub, P.T., Allen, J.S., Huyer, A., Smith, R.L., Beardsley, R.C., 1987. Seasonal cycle of currents, temperatures, winds, and sea level over the northeast Pacific continental shelf: 35°N to 48°N. Journal of Geophysical Research 92, 1507–1526.

Swallow, J.C., Molinari, R.L., Bruce, J.G., Brown, O.B., Evans, R.H., 1983. Development of near-surface flow pattern and water mass distribution in the Somali Basin in response to the Southwest Monsoon of 1979. Journal of Physical Oceanography 13, 1398–1415.

Tai, C.-K., White, W., 1990. Eddy variability in the Kuroshio extension as revealed by Geosat altimetry: energy propagation away from the jet, Reynolds stress, and seasonal cycle. Journal of Physical Oceanography 20, 1761–1777.

Talley, L.D., 1983. Radiating instabilities in thin baroclinic jets. Journal of Physical Oceanography 13, 2161–2181.

White, M.A., Heywood, K.J., 1995. Seasonal and interannual changes in the North Atlantic subpolar gyre from GEOSAT and TOPEX/POSEIDON altimetry, Journal of Geophysical Research 101, 24 931–24 942.

Willebrand, J., 1978. Temporal and spatial scales of the wind field over the North Pacific and North Atlantic. Journal of Physical Oceanography 8, 1080–1094.

Willebrand, J., Philander, S.G.H., Pacanowski, R.C., 1980. The oceanic response to large-scale atmospheric disturbances. Journal of Physical Oceanography 10, 411–429.

Wunsch, C., 1997. The vertical partition of horizontal kinetic energy and the spectrum of global variability. Journal of Physical Oceanography 27, 1770–1794.

Wunsch, C., Stammer, D., 1995. The global frequency-wavenumber spectrum of oceanic variability estimated from TOPEX/POSEIDON altimetric measurements. Journal of Geophysical Research 100, 24 895–24 910.

Wunsch, C., Stammer, D., 1998. Satellite altimetry, the marine geoid and the oceanic general circulation. Annual Reviews of Earth Planetary Sciences 26, 219–253.

Zlotnicki, V., 1991. Sea level differences across the Gulf Stream and Kuroshio extension. Journal of Physical Oceanography 21, 599–609.